Front. Mech. Eng. 2023, 18(4): 43
https://doi.org/10.1007/s11465-023-0759-x

RESEARCH ARTICLE

Improved minimum variance distortionless response spectrum method for efficient and robust non-uniform undersampled frequency identification in blade tip timing

Ruochen JIN[a], Laihao YANG (✉)[a,b], Zhibo YANG (✉)[a], Shaohua TIAN[a], Guangrong TENG[c], Xuefeng CHEN[a]

[a] *The National Key Laboratory of Aerospace Power System and Plasma Technology, Xi'an Jiaotong University, Xi'an 710049, China*
[b] *The Higher Educational Key Laboratory for Flexible Manufacturing Equipment Integration of Fujian Province, Xiamen Institute of Technology, Xiamen 361021, China*
[c] *Sichuan Gas Turbine Establishment Aero Engine Corporation of China, Mianyang 621000, China*

✉ *Corresponding authors. E-mails: yanglaihao@xjtu.edu.cn (Laihao YANG); phdapple@mail.xjtu.edu.cn (Zhibo YANG)*

ABSTRACT The noncontact blade tip timing (BTT) measurement has been an attractive technology for blade health monitoring (BHM). However, the severe undersampled BTT signal causes a significant challenge for blade vibration parameter identification and fault feature extraction. This study proposes a novel method based on the minimum variance distortionless response (MVDR) of the direction of arrival (DoA) estimation for blade natural frequency estimation from the non-uniformly undersampled BTT signals. First, based on the similarity between the general data acquisition model for BTT and the antenna array model in DoA estimation, the circumferentially arranged probes on the casing can be regarded as a non-uniform linear array. Thus, BTT signal reconstruction is converted into the DoA estimation problem of the non-uniform linear array signal. Second, MVDR is employed to address the severe undersampling issue and recover the BTT undersampled signal. In particular, spatial smoothing is innovatively utilized to enhance the estimation of covariance matrix of the BTT signal to avoid ill-condition or singularity, while improving efficiency and robustness. Lastly, numerical simulation and experimental testing are employed to verify the validity of the proposed method. Monte Carlo simulation results suggest that the proposed method behaves better than conventional methods, especially under a lower signal-to-noise ratio condition. Experimental results indicate that the proposed method can effectively overcome the severe undersampling problem of BTT signal induced by physical limitations, and has a strong potential in the field of BHM.

KEYWORDS blade tip timing (BTT), frequency identification, minimum variance distortionless response (MVDR), undersampled, blade health monitoring (BHM)

1 Introduction

Modern aircraft are pursuing superior performance and low operation and maintenance costs. In engine operation, potential faults can be found by monitoring the health condition of engine components to reduce high maintenance and avoid unnecessary downtime. Rotating blades, as a high failure-rate part of the engine, often suffer from extreme conditions, such as aerodynamic excitation, rubbing, and foreign object damage, which easily lead to fatigue accidents [1–3]. This type of damage will further cause blade cracks, blade-off faults, and other failures, eventually resulting in serious accidents of the aero-engine. Therefore, blade health monitoring (BHM) should be carried out to ensure aero-engine safety.

Blade vibration analysis and monitoring, one of the most efficient and adopted methods for BHM, has attracted extensive attention in engineering and academics. Many rotating blade condition monitoring

Received December 14, 2022; accepted May 22, 2023

methods have been proposed recently [4–6]. However, contact measurement methods, such as strain gauges [7], are limited by the disadvantages of cumbersome installation and short service life owing to the high-speed rotation of blades. Blade tip timing (BTT) [8,9], as a non-contact method of blade vibration measurement, effectively avoids the shortcomings of contact measurement. By comparing the difference between the actual arrival time when the blade vibrates and the expected arrival time without blade vibration, the blade's vibration displacement when it passes through the probe can be calculated. By installing a few sensors (3–5), the vibration of all blades in one rotor stage of the engine can be effectively estimated [10]. However, the quantity of probes is often confined owing to the physical space limitation for the BTT sensor installation on the casing, further contributing to the severe undersampling property of BTT signals. For most cases, the sampling frequency of BTT is considerably lower than the blade vibration frequency.

To solve the frequency aliasing problem caused by severe undersampling, many methods have been proposed and some decent results have been achieved [11]. Campbell [12] first used magnetic induction sensors to measure the natural frequency of rotating blades. For the early single-parameter method [13] and double-parameter method [14], a simplified dynamic model of the blade is often needed for blade vibration analysis. Moreover, only the synchronous resonance frequency can be identified through the two methods because their implementation needs the blade rotating speed passing through critical speed. Some methods, such as autoregression [15] and circumferential Fourier fitting [16], also have some limitations, including sensor installation position and parameterized prior. The "5 + 2" method [17] combines five and three probes (they share one sensor) uniformly arranged and creatively carry out blade vibration analysis using the Chinese remainder theorem. However, the requirement of seven sensors limits the application and further development of this method. Thereafter, many non-parametric methods in the fields of direction of arrival (DoA) estimation and compressed sensing were introduced into the analysis of BTT signals. Given that strong prior knowledge is avoided for these methods, the integrity of the blade vibration spectrum can be searched, so that synchronous resonance and asynchronous resonance parameters can be identified [18]. Compressed sensing theory proposed by Donoho [19] has been proven to provide excellent performance for under-sampled signal reconstruction; thus, it is widely applied to radar, communication, signal super-resolution reconstruction, and other fields. Compressed sensing also provides new possibilities for BTT. Lin et al. [20] introduced compressed sensing to the signal reconstruction of BTT. Thereafter, many scholars have attempted to further improve the performance of compressed sensing methods for BTT. Wu et al. [21] improved the sparsity of the reconstructed frequency spectrum by weighing the 1-norm regularization term. Li et al. [22] improved the iterative reweighted least squares periodogram by introducing prior knowledge to reduce computational complexity. They also verified the effectiveness of the algorithm by using experimental data. Chen et al. [23] proposed a stable BTT spectrum identification method by integrating multiple signal classification (MUSIC) and multi-bandwidth interpolation. Dong et al. [24] proposed a pursuit subspace algorithm to solve the problem of identifying synchronous vibration in BTT signal.

Considering the mechanism of BTT, some array signal model estimated using DoA is introduced to BTT signal processing because of the physical and mathematical similarity of DoA and BTT signals. For example, several classical algorithms of DoA estimation, including minimum variance distortionless response (MVDR) spectrum [18,25], MUSIC [26,27], and estimation of signal parameters via rotational invariance techniques (ESPRIT) [28], are used as nonparametric methods to estimate blade vibration spectrum. MVDR has been applied to the analysis of tip timing signals for a long time because of its high resolution and anti-aliasing property. However, the inevitable high-order matrix inversion and iterative operation result in MVDR becoming considerably time-consuming for high computational complexity, which leads to difficulty in practical applications. Although the MUSIC method has the advantages of fast calculation speed and high accuracy of spectrum estimation, the asynchronous vibration frequency could be effectively estimated only when the rotating speed approaches the resonance region. The current study proposes a BTT signal reconstruction method based on MVDR (i.e., improved minimum variance distortionless response (IMVDR)). The main contribution of the proposed method is to estimate the correlation matrix of BTT by spatial smoothing, which reduces calculation time and improves the robustness of the algorithm. The comparison of spectrum estimation performance with several recently proposed methods, including MVDR, is carried out in the simulation and experiment.

The remainder of this paper is organized as follows. Section 2 introduces the main principle of the BTT measurement. Section 3 describes the proposed method. Section 4 compares the performance of several algorithms, including MVDR, with the simulation data to verify the improvement of the proposed method. Section 5 uses a set of real experimental data to further validate the effectiveness of the proposed IMVDR method. Section 6 summarizes the main results obtained and briefly explains the limitations of the proposed method.

2 BTT measurement

The BTT measurement method is an advanced non-contact online monitoring method of blade vibration, and its schematic is shown in Fig. 1. The mainstream BTT measurement method relies on the time of arrival (ToA) probes installed on the casing to monitor the vibration of blades and the once per revolution (OPR) probes installed near the rotating shaft to calibrate the rotating speed. When the blade passes through the sensor, the light intensity received by the optical probe will suddenly change, producing a pulse, which will be transmitted to the signal acquisition system and converted from the original optical signal to the digital signal. When the blade is completely free of vibration, the expected arrival time t_{exp} of the blade in the qth probe at the N_{r}th revolution can be expressed as follows:

$$t_{\mathrm{exp}} = \frac{\theta_q + 2\pi N_{\mathrm{r}}}{2\pi f_{\mathrm{r}}(t_{\mathrm{exp}})}, \tag{1}$$

where $f_{\mathrm{r}}(t_{\mathrm{exp}})$ represents the blade's instantaneous rotation frequency at the arrival time t_{exp} and θ_q is the installation angle of the qth probe. With several circumferentially installed probes, the actual arrival time t_{act} of the blade can be measured. When the blade rotates at a high speed, its vibration will cause the lead or lag of the time instant when the blade reaches the tip timing sensor compared with that in the condition without blade vibration. Thus, the actual arrival time t_{act} can be defined as follows:

$$t_{\mathrm{act}} = \frac{\theta_q + 2\pi N_{\mathrm{r}} + x(t_{\mathrm{act}})/R}{2\pi f_{\mathrm{r}}(t_{\mathrm{act}})}, \tag{2}$$

where $x(t_{\mathrm{act}})$ is the vibration displacement of the blade at the arrival time t_{act} and R is the radius where the probe measures. The probe installed near the shaft returns one OPR pulse each time the mark passes. Thereafter, the blade rotation frequency at the N_{r}th revolution is obtained according to the time interval $T_{N_{\mathrm{r}}}$ of the adjacent pulses. The assumption is that the rotating speed of the blade changes gradually (i.e., the rotating speed does not change in each revolution), thereby simplifying the calculation of vibration displacement. The relationship between blade vibration displacement and blade arrival time can be expressed as follows:

$$x(t_{\mathrm{act}}) = 2\pi R \bar{f}_{\mathrm{r}}(N_{\mathrm{r}})(t_{\mathrm{exp}} - t_{\mathrm{act}}) = \frac{2\pi R}{T_{N_{\mathrm{r}}}}(t_{\mathrm{exp}} - t_{\mathrm{act}}), \tag{3}$$

where $\bar{f}_{\mathrm{r}}(N_{\mathrm{r}})$ represents the blade averaged rotation frequency at the N_{r}th revolution. In general, only 3 to 5 probes will be installed, and the corresponding BTT Nyquist rate is equal to $3\bar{f}_{\mathrm{r}}(N_{\mathrm{r}})$ to $5\bar{f}_{\mathrm{r}}(N_{\mathrm{r}})$, which is considerably lower than the natural frequency of the blade. To improve the sampling performance, the probes are not uniformly arranged. Therefore, sampling of the BTT signal is restricted by undersampling and non-uniform.

3 IMVDR spectrum

The relationship between array signal processing and BTT signal analysis can be established according to the basic principle of BTT sampling. Thereafter, MVDR is introduced as an effective method to reconstruct BTT signal. However, it is restricted by the time-consuming operation in autocorrelation matrix estimation, so spatial smoothing is used to improve the computational efficiency and robustness of the algorithm.

3.1 DoA estimation for BTT signal frequency identification

The contrast relationship between DoA and BTT is shown in Figs. 2(a) and 2(b). If one BTT probe per

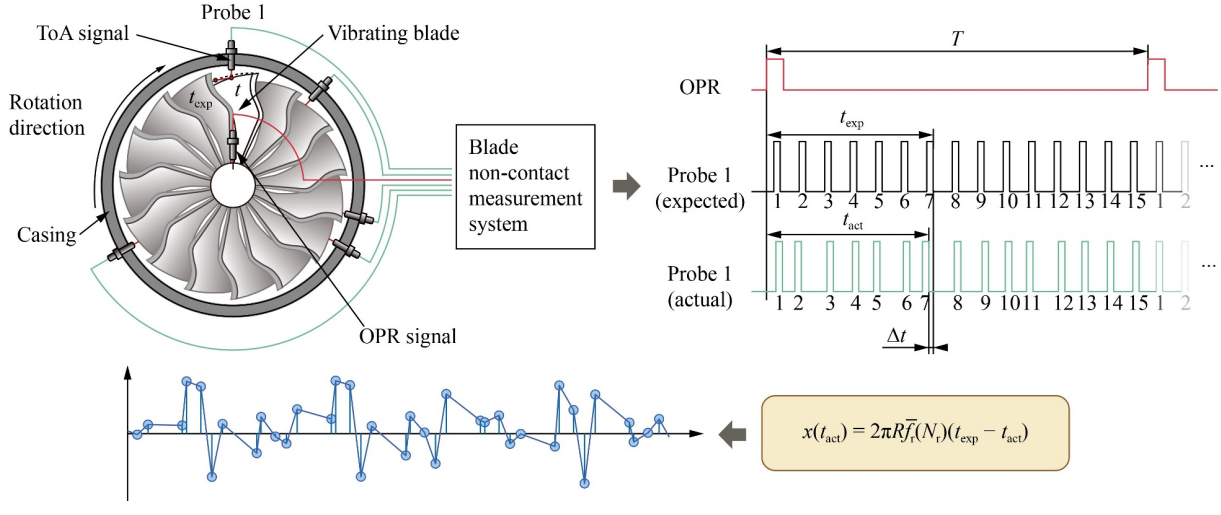

Fig. 1 Schematic of the blade non-contact measurement system for blade tip timing. OPR: once per revolution, ToA: time of arrival.

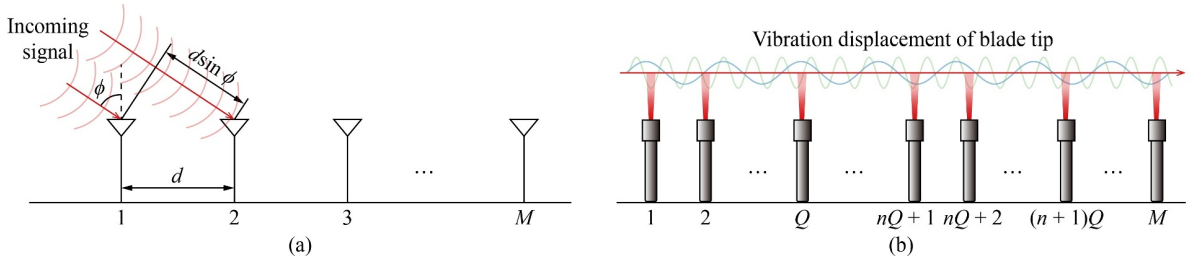

Fig. 2 (a) Antenna array model of direction of arrival and (b) linear probe array model of blade tip timing.

revolution is regarded as an independent array element, then the BTT sensors arranged in the circumferential direction can be equivalent to a one-dimensional non-uniform signal receiving array. The DoA estimation problem has a phase difference between arrays owing to the difference in the wave path between signals arriving at different array elements. The signal direction can be estimated according to the difference in wave path, and the same is true for BTT. The different time for the blade to pass through each sensor forms the phase difference of the vibration signal. An important difference between them is that the sampling rate in the DoA estimation is higher than that of the estimated signal. Moreover, the frequency of the estimated narrowband signal (i.e., center frequency ω_0) is known, while the frequency and phase of the blade vibration signal in BTT are unknown. Several DoA estimation algorithms, including MUSIC, ESPRIT, and MVDR, can be applied to the analysis of BTT undersampled signal because of their similarities.

The maximum likelihood method, which is also known as MVDR, was originally introduced by Capon [29] for wave-number analysis with large seismic arrays, and it can be adapted to single time-series spectral analysis. Lacoss [30] derived Capon's method and proved that this method is a minimum variance unbiased frequency estimator. The weight coefficient obtained using MVDR can minimize the output power of the array in the desired direction and maximize the signal-to-interference-plus-noise ratio. MVDR, as a non-parametric method, is widely used in spatial–spectral estimation and beamforming [31]. MVDR has also been applied to spectrum estimation of BTT signal in Ref. [25]. However, it involves matrix inversion and iterative operation when estimating the autocorrelation matrix of the input signal, leading to highly computational complexity and low efficiency. The current study improves MVDR to achieve high computation speed and noise robustness, while the frequency estimation accuracy of MVDR is retained. Before further comparison, deviations, development, and improvement between the proposed method and MVDR will be briefly described.

3.2 MVDR spectrum

MVDR can be regarded as a filter bank design problem, in which the final filter bank is constrained by the minimum distortion. The bandpass filters of MVDR are time and frequency dependent, which is different from the spectrum method based on a discrete Fourier matrix. Let a discrete-time signal $x(t_n)$ pass through a linear causal narrowband filter $\boldsymbol{w}$, in which signal $y(t_n)$ is denoted as the output of the filter:

$$y(t_n)=\sum_{i=0}^{M-1} w(i)\,x(t_{n+i})=\boldsymbol{w}^{\mathrm{H}}\boldsymbol{x}(t_n), \tag{4}$$

where M is the length of the $\boldsymbol{x}(t_n)$, $\boldsymbol{w}=[w(0)\quad w(1)\quad\cdots\quad w(M-1)]^{\mathrm{T}}$ is the impulse response of the filter, $(\cdot)^{\mathrm{H}}$ denotes Hermite transpose, and $\boldsymbol{x}(t_n)=[x(t_n)\quad x(t_{n+1})\quad\cdots\quad x(t_{n+M-1})]^{\mathrm{T}}$ is the input signal vector. The power of output signal $y(t_n)$ is as follows:

$$E\left\{|y(t_n)|^2\right\}=E\left\{\left|\boldsymbol{w}^{\mathrm{H}}\boldsymbol{x}(t_n)\right|^2\right\}=\boldsymbol{w}^{\mathrm{H}}\boldsymbol{R}_{xx}\boldsymbol{w}, \tag{5}$$

where $\boldsymbol{R}_{xx}$ is an $M\times M$ autocorrelation matrix of the input signal $\boldsymbol{x}(t_n)$ and $E\{\cdot\}$ is the mathematical expectation. Filter coefficients should be constrained by the idea that the response of the filter at tentative frequency f is normalized to unity:

$$\sum_{i=0}^{M-1} w(i)\,a(t_i)=\boldsymbol{w}^{\mathrm{H}}\boldsymbol{a}=1, \tag{6}$$

where $\boldsymbol{a}=[a(t_0)\quad a(t_1)\quad\cdots\quad a(t_{M-1})]^{\mathrm{T}}$ is the steering vector satisfying $\boldsymbol{a}^{\mathrm{H}}\boldsymbol{a}=\boldsymbol{a}\boldsymbol{a}^{\mathrm{H}}=1$. The input signal $\boldsymbol{x}(t_n)$ pass through filter $\boldsymbol{w}$, and there is no distortion along vector $\boldsymbol{a}$. Meanwhile, signals along other vectors tend to be attenuated. Such conditions can be expressed as minimization problems in vector form:

$$\begin{aligned}&\min_{\boldsymbol{w}}\ \boldsymbol{w}^{\mathrm{H}}\boldsymbol{R}_{xx}\boldsymbol{w},\\ &\text{s.t.}\ \ \boldsymbol{w}^{\mathrm{H}}\boldsymbol{a}=1.\end{aligned} \tag{7}$$

Equation (7) can be solved using the Lagrange multiplier method, and the optimal filter coefficients of Eq. (2) can be solved as follows:

$$\hat{\boldsymbol{w}}(\boldsymbol{a})=\frac{\boldsymbol{R}_{xx}^{-1}\boldsymbol{a}}{\boldsymbol{a}^{\mathrm{H}}\boldsymbol{R}_{xx}^{-1}\boldsymbol{a}}. \tag{8}$$

The spectrum of the input signal is defined as $\hat{\boldsymbol{w}}^{\mathrm{H}}\boldsymbol{x}(t_n)$. The simple form of MVDR can be obtained by directly replacing $\boldsymbol{w}$ in Eq. (5).

$$P_{xx}(\boldsymbol{a})=\frac{1}{\boldsymbol{a}^{\mathrm{H}}\boldsymbol{R}_{xx}^{-1}\boldsymbol{a}}. \tag{9}$$

According to the blade dynamic characteristics, blade vibration signal can be sparsely expressed in the frequency domain. Therefore, the input signal vector $\boldsymbol{x}(t_n)$ can be specifically reformulated as follows:

$$\boldsymbol{x}(t_n)=\begin{bmatrix}1 & 1 & \cdots & 1\\ \mathrm{e}^{\mathrm{j}2\pi f_0' t_1} & \mathrm{e}^{\mathrm{j}2\pi f_1' t_1} & \cdots & \mathrm{e}^{\mathrm{j}2\pi f_{m-1}' t_1}\\ \vdots & \vdots & & \vdots\\ \mathrm{e}^{\mathrm{j}2\pi f_0' t_{M-1}} & \mathrm{e}^{\mathrm{j}2\pi f_1' t_{M-1}} & \cdots & \mathrm{e}^{\mathrm{j}2\pi f_{m-1}' t_{M-1}}\end{bmatrix}\cdot\begin{bmatrix}s_0\mathrm{e}^{\mathrm{j}2\pi f_0' t_n+\mathrm{j}\varphi_0}\\ s_1\mathrm{e}^{\mathrm{j}2\pi f_1' t_n+\mathrm{j}\varphi_1}\\ \vdots\\ s_{m-1}\mathrm{e}^{\mathrm{j}2\pi f_{m-1}' t_n+\mathrm{j}\varphi_{m-1}}\end{bmatrix}+\boldsymbol{n}(t_n), \tag{10}$$

or more compactly as follows:

$$\boldsymbol{x}(t_n)=\boldsymbol{A}_x\boldsymbol{s}(t_n)+\boldsymbol{n}(t_n), \tag{11}$$

where $\boldsymbol{A}_x$ is a steering matrix for signal measurement, $\boldsymbol{s}(t_n)$ is a vector with elements composed of each frequency component at time t_n, $\boldsymbol{n}(t_n)$ is the $m\times 1$ zero-mean additive noise vector, and $\{s_0,s_1,\ldots,s_{m-1}\}$, $\{f_0',f_1',\ldots,f_{m-1}'\}$, and $\{\varphi_0,\varphi_1,\ldots,\varphi_{m-1}\}$ are the amplitude, frequency, and phase, respectively, of the blade tip vibration. According to computational accuracy, the frequency estimation range and grid with the resolution are also determined. The assumption is that the actual frequency $\{f_0',f_1',\ldots,f_{m-1}'\}$ is considered to coincide with the frequency grid, and the error caused by the mismatch between them is not considered. With the discrete frequency gridding from f_0 to f_{K-1}, the steering matrix for signal recovery could be rewritten as follows: $\boldsymbol{A}=[\boldsymbol{a}_{f_0}\ \ \boldsymbol{a}_{f_1}\ \ \cdots\ \ \boldsymbol{a}_{f_{K-1}}]$. Column $\boldsymbol{a}_f=[\mathrm{e}^{\mathrm{j}2\pi f t_n}\ \ \mathrm{e}^{\mathrm{j}2\pi f t_{n+1}}\ \ \cdots\ \ \mathrm{e}^{\mathrm{j}2\pi f t_{n+M-1}}]^{\mathrm{T}}$ of the array steering matrix $\boldsymbol{A}$ is equivalent to the complex exponential signal of the frequency f sampled by the time sequence $\boldsymbol{t}_n=[\,t_n\ \ t_{n+1}\ \ \cdots\ \ t_{n+M-1}\,]^{\mathrm{T}}$ in the BTT signal. By considering the frequencies in the range $\{f_0,f_1,\ldots,f_{K-1}\}$, the general form of the MVDR spectrum for the BTT signal is expressed as follows:

$$\boldsymbol{P}_{xx}(\boldsymbol{A})=\mathrm{diag}\{P_{xx}(\boldsymbol{a}_{f_0}),P_{xx}(\boldsymbol{a}_{f_1}),\ldots,P_{xx}(\boldsymbol{a}_{f_{K-1}})\}=\boldsymbol{A}^{\mathrm{H}}\boldsymbol{R}_{xx}\boldsymbol{W}, \tag{12}$$

where $\boldsymbol{P}_{xx}(\boldsymbol{A})$ is the diagonal matrix with diagonal elements representing the power spectral density in the range $\{f_0,f_1,\ldots,f_{K-1}\}$, that is, the MVDR spectrum of $\boldsymbol{x}(t_n)$, and $\boldsymbol{W}=[\boldsymbol{w}_0\ \ \boldsymbol{w}_1\ \ \cdots\ \ \boldsymbol{w}_{M-1}]$ is the unitary matrix with $\boldsymbol{W}^{\mathrm{H}}\boldsymbol{W}=\boldsymbol{W}\boldsymbol{W}^{\mathrm{H}}=\boldsymbol{I}$.

In practice, accurately estimating $\boldsymbol{R}_{xx}$ is difficult. In general, only the correlation matrix $\hat{\boldsymbol{R}}_{xx}$ of the sampled signal can be used as the estimation of $\boldsymbol{R}_{xx}$, which is given as $\hat{\boldsymbol{R}}_{xx}=\frac{1}{M}\boldsymbol{x}(t_n)\boldsymbol{x}^{\mathrm{H}}(t_n)$. The mutual product of average signal samples is a traditional method to obtain an autocorrelation matrix. It is not suitable for non-uniform sampling because the time interval between sampling points is not regularly distributed. In traditional MVDR [25], the autocorrelation matrix of a non-uniform signal is calculated using the Wiener-Sinchin theorem and iterative updating algorithm proposed by Liepin'sh [32].

$$\hat{\boldsymbol{R}}_{xx}^{(i+1)}=\boldsymbol{A}^{\mathrm{H}}\mathrm{diag}\left\{\hat{P}_{xx}^{(i)}(\boldsymbol{a}_{f_0}),\hat{P}_{xx}^{(i)}(\boldsymbol{a}_{f_1}),\ldots,\hat{P}_{xx}^{(i)}(\boldsymbol{a}_{f_{K-1}})\right\}\boldsymbol{A}, \tag{13}$$

$$\hat{P}_{xx}^{(i+1)}(\boldsymbol{a}_{f_k})=\left|\frac{\boldsymbol{a}_{f_k}^{\mathrm{H}}\hat{\boldsymbol{R}}_{xx}^{(i+1)-1}\boldsymbol{x}(t_n)}{\boldsymbol{a}_{f_k}^{\mathrm{H}}\hat{\boldsymbol{R}}_{xx}^{(i+1)-1}\boldsymbol{a}_{f_k}^{*}}\right|^2, \tag{14}$$

where $\hat{P}_{xx}^{(i)}(\boldsymbol{a}_{f_k})$ represents the power spectral density of tentative frequency f_k obtained at the ith iteration and $(\cdot)^*$ denotes conjugation. The peak of the MVDR spectrum appears when the steering vector is orthogonal to the noise subspace, so it can be used as a non-parametric method to identify the blade vibration frequency. Moreover, the amplitude of the spectrum obtained by MVDR represents the power of the input signal. **Algorithm 1** refers to the implementation of the MVDR spectrum for the BTT signal. The speed of MVDR is limited by three reasons: (1) non-uniform Fourier transform, (2) inversion of the large-scale matrix, and (3) iterative operation for the covariance matrix. In addition, the non-convergence of iterative operation may occur owing to only a few probes and short signal length. Note that the performance of MVDR will not be improved with an increase in signal length but with degradation. The reason is that the autocorrelation matrix will become singular or ill-conditioned. The traditional method to deal with singularity is diagonally loading a small identity matrix to make the signal covariance matrix invertible.

3.3 Spatial smoothing

To avoid simultaneous excessive calculation cost and spectrum estimation error, one-dimensional BTT signals are rearranged by spatial smoothing. Spatial smoothing is used in DoA estimation to overcome matrix rank reduction and matrix singular caused by signal coherence [33]. The input signal $\boldsymbol{x}(t_n)$ measured by probes $\{1,2,\ldots,Q\}$ is divided into $N=\lfloor(M-L)/Q\rfloor+1$ overlapping snapshots with a window length of L. The starting point of each snapshot must correspond to the same sensor to ensure the same structure. The ith snapshots $\boldsymbol{x}_i(t_n)$ is as follows:

$$\boldsymbol{x}_i(t_n)=\boldsymbol{A}_x\boldsymbol{\Lambda}^{i-1}\boldsymbol{s}(t_n)+\boldsymbol{n}(t_n), \tag{15}$$

where $\boldsymbol{\Lambda}=\mathrm{diag}\left\{\mathrm{e}^{\mathrm{j}2\pi f_0'(t_{n+Q}-t_n)},\mathrm{e}^{\mathrm{j}2\pi f_1'(t_{n+Q}-t_n)},\ldots,\mathrm{e}^{\mathrm{j}2\pi f_{m-1}'(t_{n+Q}-t_n)}\right\}$ is the diagonal matrix. Thus, the covariance matrix of the ith snapshot is obtained as follows:

$$\boldsymbol{R}_i=\boldsymbol{A}_x\boldsymbol{\Lambda}^{i-1}E\{\boldsymbol{s}(t_n)\boldsymbol{s}^{\mathrm{H}}(t_n)\}\left(\boldsymbol{\Lambda}^{i-1}\right)^{\mathrm{H}}\boldsymbol{A}_x^{\mathrm{H}}+\sigma_n^2\boldsymbol{I}. \tag{16}$$

Algorithm 1 MVDR spectrum for the BTT signal

Input: the arrival time $\boldsymbol{t}_n$, the vibration displacement $\boldsymbol{x}(\boldsymbol{t}_n)$, frequency sequence $\{f_0, f_1, \ldots, f_{K-1}\}$, max iterations $N_{\max}$, and error ε;

Output: MVDR spectrum $\left\{P_{xx}(\boldsymbol{a}_{f_0}), P_{xx}(\boldsymbol{a}_{f_1}), \ldots, P_{xx}(\boldsymbol{a}_{f_{K-1}})\right\}$;

Initialization $\hat{P}_{xx}^{(0)}(\boldsymbol{a}_{f_k}) = \left(\frac{1}{M}\boldsymbol{a}_{f_k}^{\mathrm{H}}\boldsymbol{x}(\boldsymbol{t}_n)\right)^2$, $\varepsilon = 0.05$, $i = 0$;

Obtain array steering matrix $\boldsymbol{A} = \left[\boldsymbol{a}_{f_0} \quad \boldsymbol{a}_{f_1} \quad \cdots \quad \boldsymbol{a}_{f_{K-1}}\right]$ with f_k and $\boldsymbol{t}_n$;

while $\sum_{k=0}^{K-1}\left|\hat{P}_{xx}^{(i+1)}(\boldsymbol{a}_{f_k}) / \hat{P}_{xx}^{(i)}(\boldsymbol{a}_{f_k}) - 1\right| < \varepsilon$ **and** $i < N_{\max}$ **do**

  Update $\hat{\boldsymbol{R}}_{xx}^{(i+1)}$ and $\hat{P}_{xx}^{(i+1)}(\boldsymbol{a}_{f_k})$ by Eqs. (13) and (14);

  $i = i + 1$;

end while

for $f_k \in \{f_0, f_1, \ldots, f_{K-1}\}$ **do**

  $P_{xx}(\boldsymbol{a}_{f_k}) = \dfrac{1}{\boldsymbol{a}_{f_k}^{\mathrm{H}}\hat{\boldsymbol{R}}_{xx}^{-1}\boldsymbol{a}_{f_k}^{\mathrm{H}}}$;

end for

Return: $\left\{P_{xx}(\boldsymbol{a}_{f_0}), P_{xx}(\boldsymbol{a}_{f_1}), \ldots, P_{xx}(\boldsymbol{a}_{f_{K-1}})\right\}$.

Let the covariance matrix of the input signal with spatial smoothing be rewritten as the means of snapshots:

$$\begin{aligned}\boldsymbol{R}'_{xx} &= \boldsymbol{A}_x\left(\frac{1}{N}\sum_{i=1}^{N}\boldsymbol{\Lambda}^{i-1}E\{\boldsymbol{s}(t_n)\boldsymbol{s}^{\mathrm{H}}(\boldsymbol{t}_n)\}\left(\boldsymbol{\Lambda}^{i-1}\right)^{\mathrm{H}}\right)\boldsymbol{A}_x^{\mathrm{H}} + \sigma_n^2\boldsymbol{I} \\ &= \boldsymbol{A}_x\bar{\boldsymbol{S}}\boldsymbol{A}_x^{\mathrm{H}} + \sigma_n^2\boldsymbol{I}. \end{aligned} \tag{17}$$

The spatial smoothed covariance matrix $\bar{\boldsymbol{S}}$ can be represented by a block matrix:

$$\bar{\boldsymbol{S}} = \begin{bmatrix}\boldsymbol{I} & \boldsymbol{I}\boldsymbol{\Lambda} & \cdots & \boldsymbol{I}\boldsymbol{\Lambda}^{N-1}\end{bmatrix}\begin{bmatrix}\frac{1}{N}\boldsymbol{S} & & \\ & \ddots & \\ & & \frac{1}{N}\boldsymbol{S}\end{bmatrix}\begin{bmatrix}\boldsymbol{I} \\ (\boldsymbol{I}\boldsymbol{\Lambda})^* \\ \vdots \\ \left(\boldsymbol{I}\boldsymbol{\Lambda}^{N-1}\right)^*\end{bmatrix} = \boldsymbol{G}\boldsymbol{G}^{\mathrm{H}}, \tag{18}$$

where $\boldsymbol{S} = E\{\boldsymbol{s}(\boldsymbol{t}_n)\boldsymbol{s}^{\mathrm{H}}(\boldsymbol{t}_n)\}$ is the covariance matrix of the signal vector at time $\boldsymbol{t}_n$ and $\boldsymbol{G} = [\sqrt{\boldsymbol{S}/N} \quad \boldsymbol{\Lambda}\sqrt{\boldsymbol{S}/N} \quad \cdots \quad \boldsymbol{\Lambda}^{N-1}\sqrt{\boldsymbol{S}/N}]$ is the block matrix. Note that the singularity of matrix $\bar{\boldsymbol{S}}$ is the singularity of matrix $\boldsymbol{G}$. Take the elementary transformation of matrix $\boldsymbol{G}$, and the rank of the matrix $\boldsymbol{G}$ can be expressed as follows:

$$\begin{aligned} rank(\boldsymbol{G}) &= rank\left(\begin{bmatrix} s_{11}\boldsymbol{v}_1 & s_{12}\boldsymbol{v}_1 & \cdots & s_{1m}\boldsymbol{v}_1 \\ s_{21}\boldsymbol{v}_2 & s_{22}\boldsymbol{v}_2 & \cdots & s_{2m}\boldsymbol{v}_2 \\ \vdots & \vdots & & \vdots \\ s_{m1}\boldsymbol{v}_m & s_{m2}\boldsymbol{v}_m & \cdots & s_{mm}\boldsymbol{v}_m \end{bmatrix}\right) \\ &= rank\left(\begin{bmatrix} c_1\boldsymbol{v}_1 \\ c_2\boldsymbol{v}_2 \\ \vdots \\ c_m\boldsymbol{v}_m \end{bmatrix}\right), \end{aligned} \tag{19}$$

where $rank(\cdot)$ denotes the rank of the matrix, s_{ij} is the element of the matrix $\sqrt{\boldsymbol{S}/N}$ in row i and column j, $\boldsymbol{v}_i = [\boldsymbol{1} \quad \boldsymbol{\Lambda}_{ii}^1 \quad \cdots \quad \boldsymbol{\Lambda}_{ii}^{N-1}]$ is the ith row of a Vandermonde matrix, and c_i is any non-zero element in the ith row of the matrix $\sqrt{\boldsymbol{S}/N}$. Given that $\boldsymbol{S}$ is the amplitude of the input signal, there are always non-zero elements in each row (i.e., c_i always exists). When the number of subarrays N is higher than the number of frequency components m, the Vandermonde matrix is evidently full row rank. Consequently, matrix $\boldsymbol{G}$ is full row rank and covariance matrix $\boldsymbol{R}'_{xx}$ is non-singular.

Although spatial smoothing ameliorates the singularity

and ill-condition, the frequency resolution of the proposed method is reduced owing to subarray division. However, this compromise will be verified to be reasonable, thereby improving the robustness of the algorithm and also has advantages in processing the BTT data in the non-resonance region. Figure 3 shows the schematic of the proposed method. The main steps of IMVDR are summarized in **Algorithm 2**.

The computational complexity of IMVDR mainly comes from the inversion of the autocorrelation matrix and calculation of spectrum, which are $O(M^3)$ and $O(KM^2)$, respectively. The computational complexity of

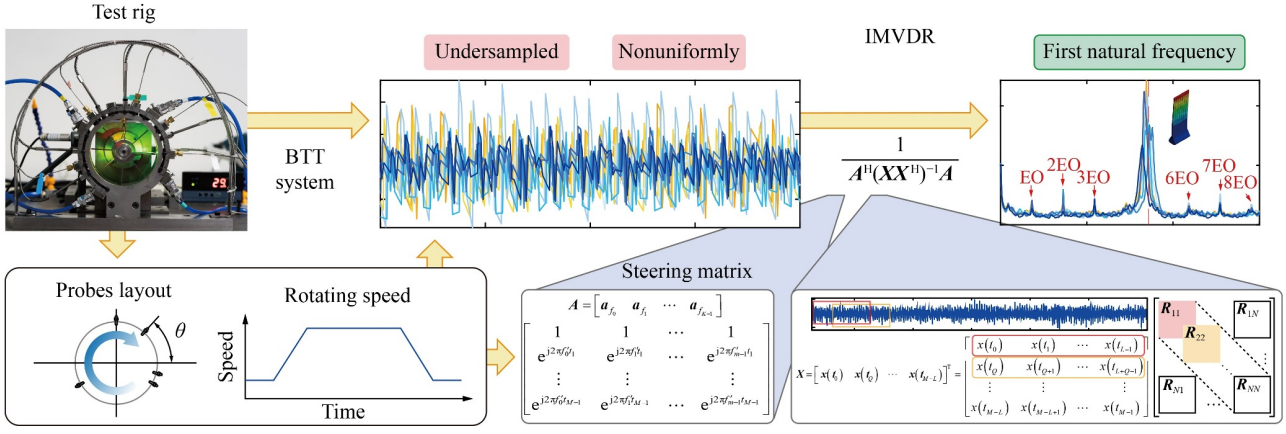

Fig. 3 Schematic of the proposed improved minimum variance distortionless response (IMVDR). BTT: blade tip timing.

Algorithm 2 IMVDR spectrum for the BTT signal

Input: the arrival time $\boldsymbol{t}_n$, the vibration displacement $\boldsymbol{x}(\boldsymbol{t}_n)$, frequency sequence $\{f_0, f_1, \ldots, f_{K-1}\}$, length of the snapshot L, length of the signal M, and number of probes Q;

Output: IMVDR spectrum $\left\{P_{xx}(\boldsymbol{a}_{f_0}), P_{xx}(\boldsymbol{a}_{f_1}), \ldots, P_{xx}(\boldsymbol{a}_{f_{K-1}})\right\}$;

Obtain array steering matrix $\boldsymbol{A} = \left[\boldsymbol{a}_{f_0} \quad \boldsymbol{a}_{f_1} \quad \ldots \quad \boldsymbol{a}_{f_{K-1}}\right]$ with f_k and $\boldsymbol{t}_n$;

Calculate the number of snapshots $N = \lfloor (M-L)/Q \rfloor + 1$;

for $i = 0 : N-1$ **do**

    $\boldsymbol{x}_i(\boldsymbol{t}_n) = \boldsymbol{x}(\boldsymbol{t}_n)[i \times Q : i \times Q + L]$;

end for

Calculate the correlation matrix $\hat{\boldsymbol{R}}_{xx} = \frac{1}{N}\sum_{i=1}^{N} \boldsymbol{x}_i(\boldsymbol{t}_n)\boldsymbol{x}_i^{\mathrm{H}}(\boldsymbol{t}_n)$;

for $f_k \in \{f_0, f_1, \ldots, f_{K-1}\}$ **do**

    $P_{xx}(\boldsymbol{a}_{f_k}) = \frac{1}{\boldsymbol{a}_{f_k}^{\mathrm{H}} \hat{\boldsymbol{R}}_{xx}^{-1} \boldsymbol{a}_{f_k}^{\mathrm{H}}}$;

end for

Return: $\left\{P_{xx}(\boldsymbol{a}_{f_0}), P_{xx}(\boldsymbol{a}_{f_1}), \ldots, P_{xx}(\boldsymbol{a}_{f_{K-1}})\right\}$.

MVDR is $O(N_{\text{ite}}KL^2)$, where N_{ite} is the number of iterations and usually equal to 10–20. Although matrix inversion is inevitable in IMVDR and MVDR, the dimension of the autocorrelation matrix in IMVDR is equal to the snapshot width, which is much smaller than the signal length, and it is only executed once. The aforementioned reasons make IMVDR an extremely low time-consuming method.

4 Numerical verification

This section uses a group of synthesized signals with non-uniform undersampling characteristics to preliminarily verify the anti-aliasing and amplitude estimation abilities of the proposed method. Moreover, the improvement of the proposed method and change in estimation accuracy are illustrated by comparing it with the MVDR method.

4.1 Synthetic signal

Blade vibration is mainly composed of synchronous and asynchronous resonance. Synchronous resonance is generally caused by the rotor, drive excitation, and blade crack, among others. Asynchronous resonance corresponds to surge, flutter, and other fault phenomena. Therefore, synchronous resonance is an integer multiple of rotational speed, whereas asynchronous resonance is non-integer. This difference is manifested in the time domain: the former is measured in the same phase by BTT probes, while the latter is measured in different phases [34]. Hence, the synthetic signal containing synchronous and asynchronous resonance can be expressed as follows:

$$\begin{aligned} x(t) &= \sum_{i=1}^{3} a_i \mathrm{e}^{\mathrm{j}2\pi f_i t} + w(t), \\ f &= \begin{bmatrix} 100.0 & 246.7 & 333.3 \end{bmatrix} \mathrm{Hz}, \\ a &= \begin{bmatrix} 1.00 & 2.00 & 1.50 \end{bmatrix}, \end{aligned} \tag{20}$$

where function $w(t)$ is the Gaussian white noise. Blade rotation speed is assumed to be 4000 r/min, and the installation angle of five BTT probes is [0°, 36°, 78°, 156°, 282°]. The undersampled signal (orange cross) obtained by five BTT probes is shown in Fig. 4(a). As shown in Fig. 4(b), the direct use of non-uniform Fourier transform (NUFT) will cause serious frequency aliasing, and the correct frequency components cannot be identified.

1) IMVDR vs. MVDR. The results obtained by MVDR and IMVDR are shown in Fig. 5, where the red square indicates the ground truth. The comparative results indicate that IMVDR is more effective and robust than MVDR for the vibration reconstruction of the undersampled signal. Moreover, calculation speed is improved, while the estimation accuracy of the spectrum is maintained. As shown in Fig. 5(a), when the grid size is 1 Hz, the MVDR method has a frequency mismatch, leads to a substantial decline in estimation accuracy. This influence is reflected in the increase of amplitude estimation error in the IMVDR method. With an increase in grid size, the performances of MVDR and IMVDR can be improved, and a more evident improvement can be observed in the estimation results obtained using IMVDR. Note that apart from frequency, amplitude is also more accurately estimated through IMVDR under a grid size of 0.1 Hz, as shown in Figs. 5(d)−5(f). Meanwhile, MVDR may lead to less amplitude identification accuracy, as shown in Fig. 5. In generally speaking, the improvement of IMVDR in the analysis of the spectrum of non-uniform undersampled signal is effective compared with the traditional MVDR method. Furthermore, the amplitude obtained by IMVDR is certainly valuable, but the higher accuracy of amplitude estimation corresponds to a finer grid, which also corresponds to longer calculation time.

2) The influences of snapshot width, signal length, noise level, and frequency resolution are quantitatively analyzed, and the comparative results are shown in Fig. 6. Figures 6(a) and 6(b) show the approximate parameter selection range. The estimation accuracy will decrease with an increase of snapshot width, but the best estimation result is achieved when L = 32. As shown in Fig. 6(c), with a decrease in signal-to-noise ratio (SNR), the estimation accuracy of the signal frequency is not

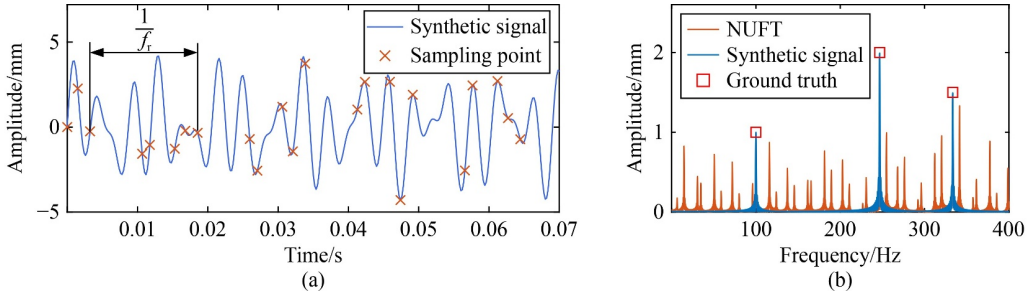

Fig. 4 Synthetic blade tip timing (BTT) simulation signal: (a) original signal and BTT sampling points and (b) non-uniform Fourier transform (NUFT) of the undersampled signal.

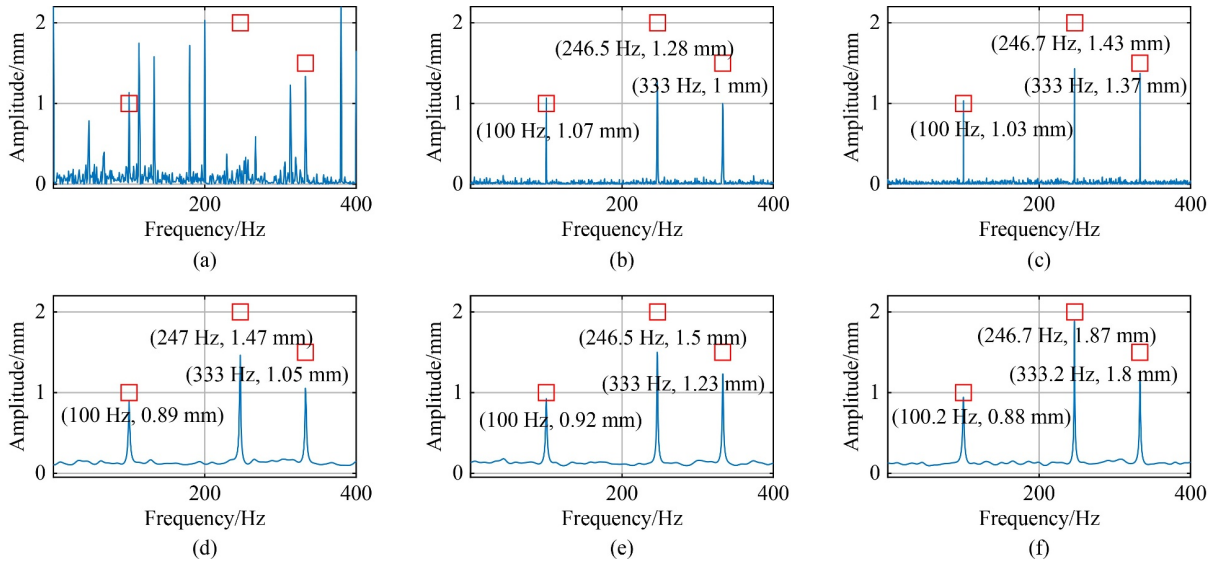

Fig. 5 Minimum variance distortionless response (MVDR) spectrum estimation results of the synthetic blade tip timing simulation signals (M = 512, L = 16) with resolutions of (a) 1 Hz (0.018 s), (b) 0.5 Hz (0.0598 s), and (c) 0.1 Hz (1.0962 s). Improved MVDR spectrum estimation results of the synthetic blade tip timing simulation signals (M = 512, N_{ite} = 15) with resolutions of (d) 1 Hz (4.2549 s), (e) 0.5 Hz (6.0917 s), and (f) 0.1 Hz (67.1167 s).

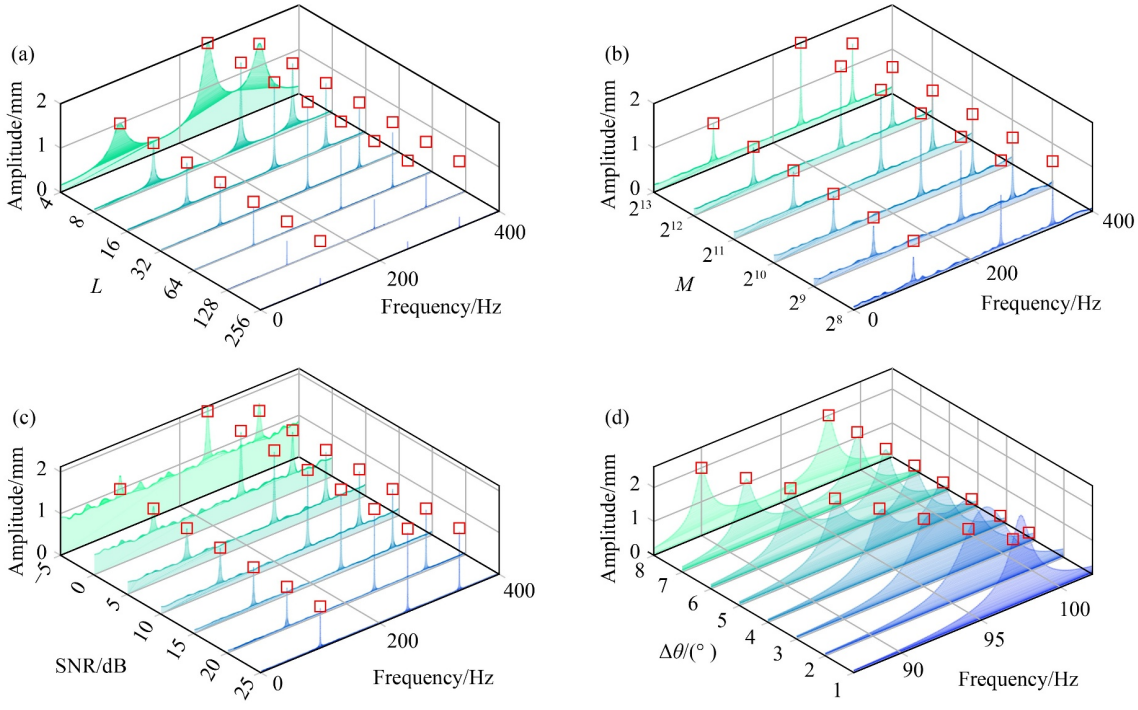

Fig. 6 Relationship between improved minimum variance distortionless response (IMVDR) spectrum and different conditions: (a) IMVDR spectrum and snapshots width L, (b) IMVDR spectrum and signal length M, (c) IMVDR spectrum and signal-to-noise ratio (SNR), and (d) IMVDR spectrum and minimum frequency interval $\Delta\theta$.

affected. However, note that as SNR continues to decrease, the estimation accuracy of the signal amplitude is reduced, especially when SNR < 5 dB. Overall, the IMVDR spectrum is robust to noise, in which the robustness of frequency estimation is better than that of the amplitude. The resolution result of the IMVDR spectrum is shown in Fig. 6(d). At a sampling frequency of 90 Hz, the two frequency components of 90 and $(90+\Delta\theta)$ Hz are not considerably distinguished when $\Delta\theta < 3$ Hz. Nevertheless, this problem can be solved by increasing the input signal length M and snapshot width L.

4.2 Monte Carlo simulation

In this section, several common BTT signal spectrum estimation methods are used to compare with the proposed methods, including MUSIC [27], ESPRIT [28], MVDR [25,35], orthogonal matching pursuit (OMP) [36,37], alternating direction method of multipliers (ADMM) [38], iteratively reweighted least squares (IRLS) [39], and "5 + 2" [40,41]. MUSIC, ESPRIT, MVDR, and IMVDR are typical algorithms of DoA estimation. MUSIC uses the noise subspace of the signal, while MVDR uses the signal subspace. ESPRIT takes advantage of the rotation invariance of signal subspaces between two signal covariance matrices and directly decomposes the eigenvalue to obtain the frequency instead of the complete spectrum. OMP and ADMM belong to sparse signal recovery algorithms. OMP is a classical greedy algorithm to approximately solve the L0-norm minimization problem. The ADMM algorithm solves the Lasso problem of relaxing L0-norm to L1-norm, while IRLS is a nonparametric method for the spectral analysis of non-uniform undersampled signals. Meanwhile, "5 + 2" de-aliases undersampled signals by constructing two groups of signals with different sampling rates.

The synthesized signal with K known frequency components is used to compare the performances of several algorithms. With the exception of the ESPRIT algorithm, which directly selects the largest K eigenvalues, all other algorithms use the peak search algorithm to find the largest K peaks. Note that not all algorithms are capable of amplitude identification, so the amplitude of each frequency component is normalized to 1. Empirical root mean square error (RMSE) is selected as the index to evaluate each algorithm:

$$\mathrm{RMSE}=\sqrt{\frac{1}{N_{\mathrm{mc}}K}\sum_{k=0}^{K-1}\sum_{n=0}^{N_{\mathrm{mc}}-1}\left(\hat{f}_k^n-f_k^n\right)^2}, \tag{21}$$

where $[f_0^n, f_1^n, \ldots, f_{K-1}^n]^{\mathrm{T}}$ and $\left[\hat{f}_0^n, \hat{f}_1^n, \ldots, \hat{f}_{K-1}^n\right]^{\mathrm{T}}$ represent the ground truth of the frequencies and estimated value of the frequencies, respectively, and N_{mc} indicates the total number of testing examples for the Monte Carlo simulation.

1) RMSE vs. SNR. In this case, several randomly generated frequencies ranging in [1, 200] Hz were used. At each SNR level, Monte Carlo simulations are conducted 100 times. The input signal length of several methods is 512, in which the snapshot width of IMVDR and MUSIC is 16. The result of the Monte Carlo simulation is shown in Fig. 7. Note that at low SNR, the proposed method performs well, and its calculation time is slightly lower than that of MUSIC and considerably faster than those of other methods. The proposed IMVDR shows higher accuracy and lower calculation time compared with OMP, which can also identify amplitude.

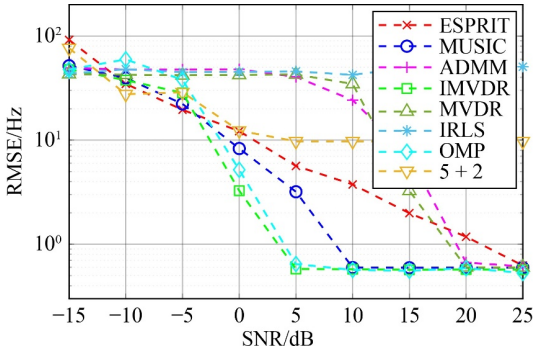

Fig. 7 Root mean square error (RSME) (logarithmic scale) vs. signal-to-noise ratio (SNR) in the different methods of spectrum estimation with two random frequency components.

The ESPRIT method, as a gridless method, is different from other methods, and its accuracy is continuously improved with the decrease of SNR. Similar to the other three on-grid methods, accuracy does not improve when SNR decreases to 5 dB owing to the limitation of the grid size. Note that this feature belongs to all types of on-grid methods, and obtaining finer grids with higher accuracy is expected. However, finer grids will lead to lower performance and higher computing time. The ADMM algorithm needs to adjust parameters λ and ρ to obtain a relatively stable performance when SNR changes. Meanwhile, other algorithms do not need to adjust parameters in the simulation process. Note also that the IRLS algorithm is extremely sensitive to the sum of the number of sensors, arrangement of sensors, and signal length, so IRLS cannot realize reasonable spectrum estimation in this Monte Carlo simulation. Moreover, "5 + 2" requires two additional probes compared with other methods. Although the spectrum obtained by "5 + 2" contains the correct frequency value, discerning the correct peak value is often challenging owing to aliasing and frequency leakage.

2) RMSE vs. input signal length. Figure 8 shows that the RMSE results of two frequencies for the length of input signal vary from 32 to 2048. The frequency range of the synthetic signal remains unchanged, and SNR of all signals is 15 dB. For each signal length M, 100 Monte Carlo simulations are carried out. When the input signal length is over 64, the frequency values estimated by IMVDR obtain the minimum RMSE, and the performance decreases slightly when length M is below 64. With an increase in input signal length, the fixed grid resolution limits the performance of all grid-based estimators except for ESPRIT. Note that compared with the influence of SNR change, ADMM is less sensitive to signal length M. Hence, ADMM does not adjust parameters λ and ρ in this MC simulation. For IRLS, although signal length has changed, RMSE of frequency is still larger than that of other methods owing to random sensor arrangement and small numbers.

5 Experimental verification

Experiments were further conducted to verify the effectiveness of the proposed IMVDR method, especially the excellent performance of the proposed method in asynchronous resonance frequency extraction. Given that there is no contact measurement system installed on the test rig, several methods that have been applied in BTT are used for reference.

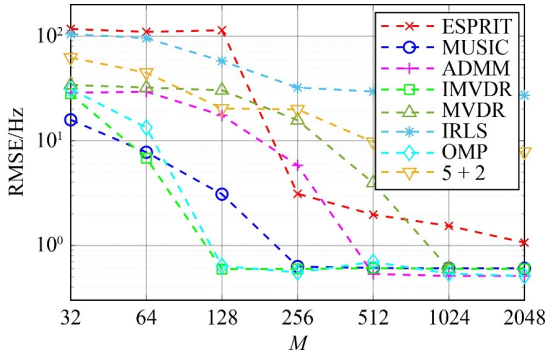

Fig. 8 RMSE (logarithmic scale) versus signal length M in the different methods of spectrum estimation with two random frequency components.

5.1 Experimental setup

In this section, a test rig (see Fig. 9) equipped with a BTT measurement system is used to collect data. An aluminum disk with eight blades is driven by a servo motor with a maximum speed of 15000 r/min. BTT probes circumferentially installed on the casing are used to measure blade vibration, and an OPR probe is used to indicate the rotation speed. Five BTT probes were installed at the position in the following angles: 48°, 108°, 158°, 168°, and 288°. Through finite element modeling (FEM) analysis, the first and second modal frequencies at different angular velocities are calculated, and the Campbell diagram of the blade is obtained as shown in Fig. 10. The red circle indicates that the first modal frequency of the blade intersects with four times

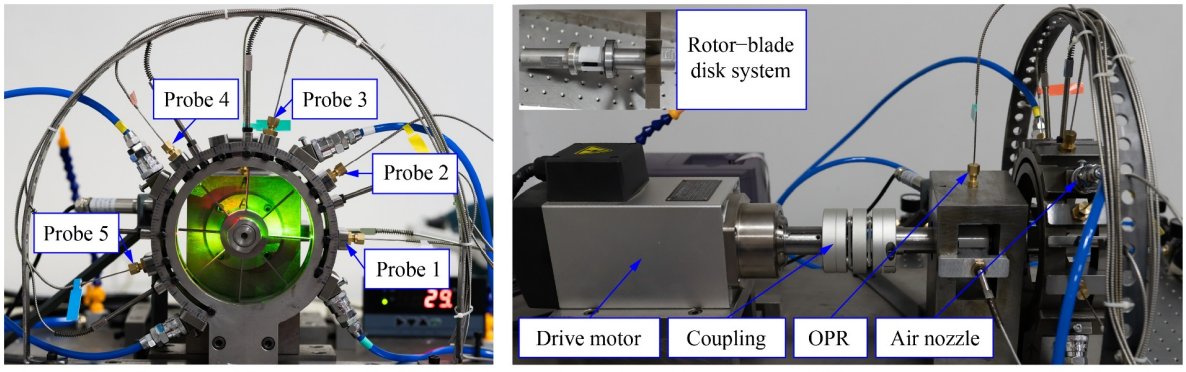

Fig. 9 Test rig of blade tip timing: (a) front view and (b) left view.

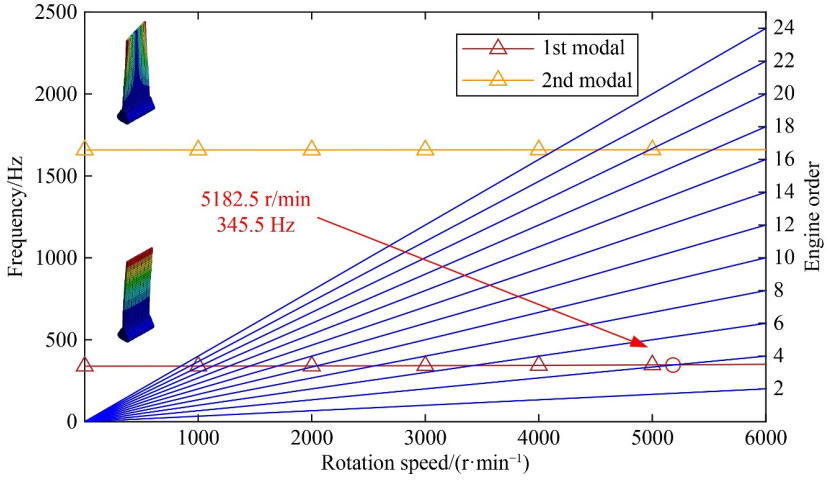

Fig. 10 Campbell diagram of the blade.

the rotation frequency of the blade, and the blade resonates at 345.5 Hz. Meanwhile, strain gauges are installed at the root of the blade. The resistance change of the strain gauge caused by blade vibration is input into data acquisition through the Wheatstone bridge. The sampling frequency of the strain gauge is 20000 Hz, which is significantly higher than the first two-order natural frequency.

Motor speed is set to the acceleration and constant speed sections. Four 0.75 MPa pneumatic excitation are applied to the blade tip to simulate the actual working condition. The BTT data of blade 1 measured in the experiment are shown in Fig. 11. As indicated in the experimental data of blade 1, several resonances occur in the acceleration, and a resonance appears at 5200 r/min, which is consistent with the FEM result of the Campbell diagram.

5.2 Data analysis

Several methods mentioned in Section 4 are used to analyze the experimental data, except for ESPRIT because it cannot obtain the complete spectrum. To better compare the performance differences among several methods, data in the resonance region are excluded. Instead, data at 48 s corresponding to the rotation speed of 4360 r/min are selected. Signal length is 1024 and frequency grid size is 1 Hz. The snapshot width used by IMVDR and MUSIC is 64, the sparsity of OMP is set to 10, 20 iterations are used for MVDR, 30 for ADMM, and 10 for IRLS. Figures 12(a) to 12(h) show that the spectra obtained by each method include the original BTT signal. The red dot line in Fig. 12 indicates the natural frequency obtained using the FEM model.

IMVDR and MUSIC reflect the natural frequency and provide remarkable anti-aliasing even in the non-resonance region. The estimated frequency is summarized in Table 1. However, the frequency spectrum obtained by MUSIC lacks amplitude and each order of rotation frequency is also lost. OMP, can only obtain each order of frequency compared with MUSIC, but the vibration caused by resonance is almost eliminated. The results given by MVDR and NUFT are markedly similar, and both have frequency errors caused by speed variation. The anti-aliasing of MVDR is better than that of NUFT, but the natural frequency in NUFT is more prominent. ADMM and IRLS are used to solve the Lasso problem, and note that the effects of these two methods on the BTT data in the non-resonance region are not ideal. Another point is that the amplitudes of several methods are meaningful except for the pseudo amplitude obtained by MUSIC. Taking blade 1 as an example, although the amplitudes of several methods are in the same order of magnitude, the maximum amplitudes differ by 0.022 mm (IMVDR, 0.032 mm, and OMP, 0.010 mm). This result also indicates that highly accurate amplitude estimation is difficult to achieve.

To compare IMVDR and MUSIC more comprehensively, the time–frequency representation of BTT signals was analyzed using the two methods. Data from blade 2 installed with strain gauge is divided into 2000 data segments of signal length is 2048, with a step size of 20. Rotation speed in each data segment is regarded as a constant to simplify calculations. Given that IMVDR, MUSIC, and strain gauge are on-grid methods, frequency grid size is set to 1 Hz. In addition, amplitudes of short time Fourier transform and IMVDR represent the estimation of the input signal amplitude, while amplitudes of MUSIC represent the orthogonality between the signal and noise subspaces. Figure 13 shows the estimation results of the spectrogram by IMVDR, MUSIC, and strain gauge. Note that the result of IMVDR is markedly better than MUSIC. In the entire time–frequency domain, the natural frequency of the blade can be identified, and the synchronous resonance of each order is still reserved. Moreover, the blade vibration amplitude is observed to increase as the rotating speed approaches the resonance region. In the results obtained by MUSIC, frequency spectrum at high speed is similar to that in Fig. 12(f), and natural frequency disappears at low speed. Moreover, the line indicating the natural frequency in MUSIC "breaks" near the resonance zone, which has been confirmed in Ref. [42]. As shown in the subplot, natural frequency is transported near the resonance region and coincides with

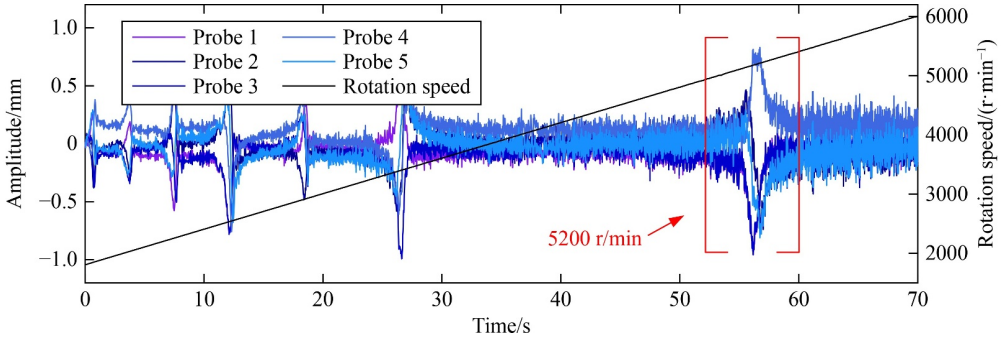

Fig. 11 Blisk rotation speed and blade tip vibration displacement of blade 1 sampled by blade tip timing system.

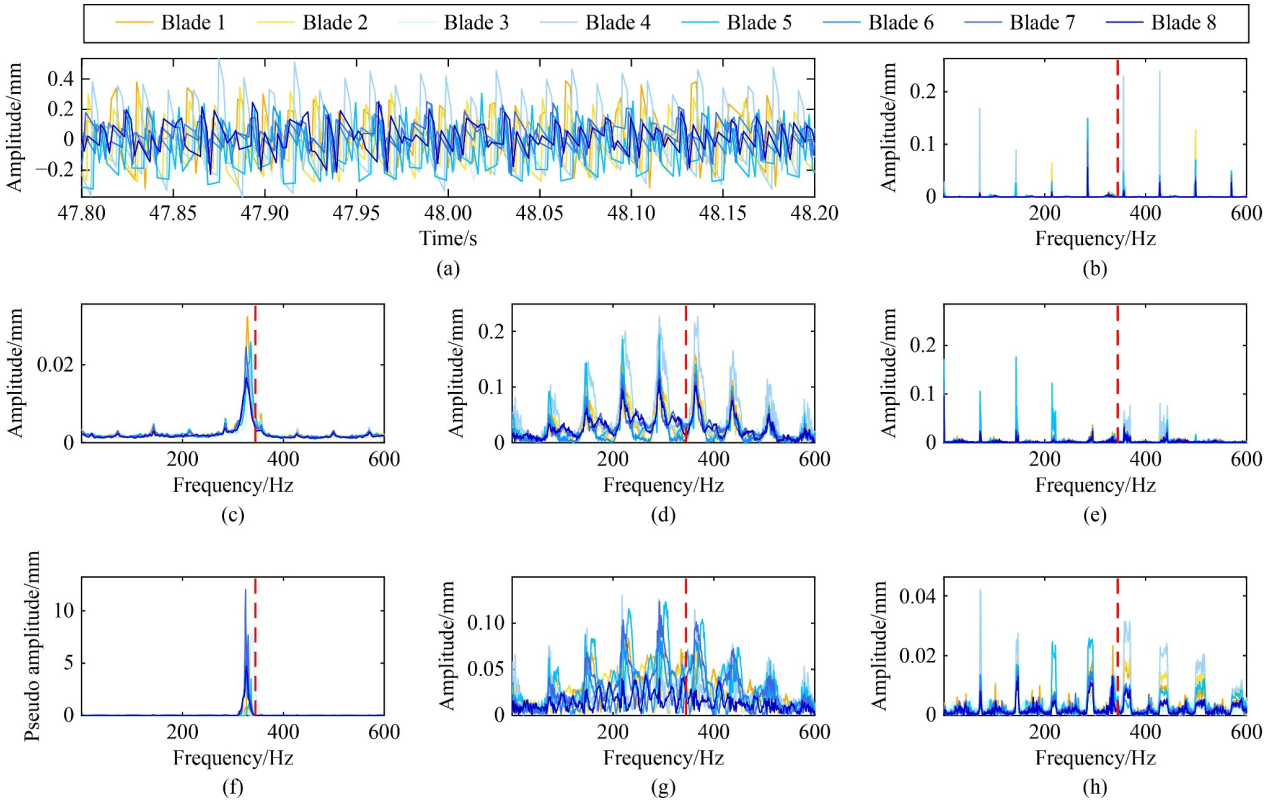

Fig. 12 Frequency spectra of 8 blade tip vibration displacement: (a) original blade tip timing sampled signal, (b) orthogonal matching pursuit, (c) improved minimum variance distortionless response, (d) iteratively reweighted least squares, (e) minimum variance distortionless response, (f) multiple signal classification, (g) alternating direction method of multipliers, and (h) non-uniform Fourier transform.

Table 1 Comparison of the blade natural frequency between IMVDR and MUSIC. Rotation speed is 4360 r/min (t = 48 s)

Method	Blade natural frequency/Hz							
	Blade 1	Blade 2	Blade 3	Blade 4	Blade 5	Blade 6	Blade 7	Blade 8
IMVDR	335	336	345	335	342	333	332	334
MUSIC	335	337	344	335	343	332	331	333

the synchronous vibration frequency. The results of strain gauge can extract the rotation frequency, natural frequency of the blade, and enhancement of four times engine order caused by the pneumatic excitation.

As shown in Fig. 13(a), the 1st order natural frequency at low speed obtained by IMVDR lies in a band. The reason is related to the basic principle that the Nyquist rate of BTT is proportional to the rotating speed of the bladed disk. The same signal length, high sampling rate, and short sampling time at high speed are observed but opposite at low speed. Rotational speed is regarded as a constant value when estimating the spectrum in each segment. Consequently, acceleration at low rotational speed leads to a significant deviation of the array steering matrix and eventually causes the frequency estimation error. Execution time takes 44.69 s for IMVDR spectrogram and 44.80 s for MUSIC, both of which are in Python 3.8. Even though IMVDR and MUSIC can achieve excellent efficiency, the estimation results obtained by IMVDR retain more information on vibration. The comprehensive compassion further demonstrates that the proposed IMVDR balances the relationship between accuracy and calculation efficiency. This result provides additional possibilities for the online monitoring of blade vibration.

6 Conclusions

BTT is a non-intrusive and non-contact blade vibration measurement method. Although limited by the Shannon sampling theorem, many effective methods have been proposed to overcome frequency aliasing. This study uses previous research as basis to improve the early MVDR method and eventually propose a more efficient IMVDR method. Furthermore, the elaborate signal matrix

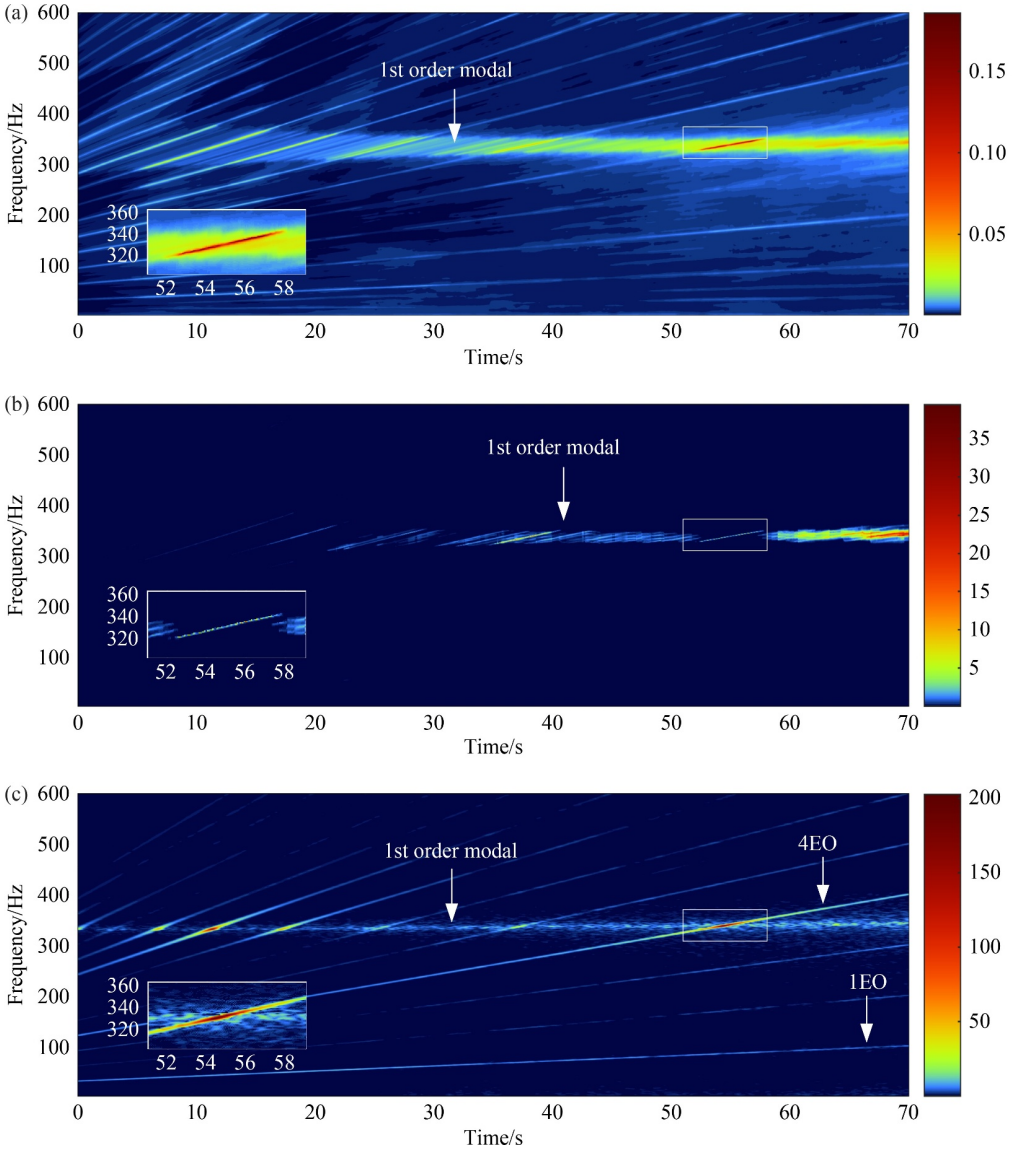

Fig. 13 Spectrogram of blade 2 tip vibration displacement: (a) improved minimum variance distortionless response, (b) multiple signal classification, and (c) strain gauge.

skillfully reduces the order of the autocorrelation matrix and avoids the iteration process. A comparison between the proposed method and other methods through simulation and experimental data is also conducted. lastly, the following conclusions are summarized and presented.

1) IMVDR is a nonparametric method that effectively solves the problem of non-uniform undersampling of BTT signal and realizes the estimation of blade vibration frequency and amplitude. Moreover, IMVDR requires less prior knowledge than the single-parameter method. Spatial smoothing is used to preprocess the estimated signal, which maintains high estimation accuracy and also avoids the inversion of the high-order matrix and iterative operation.

2) In the synthetic BTT data and MC simulation, IMVDR is compared with recently proposed methods. Results show that IMVDR has noise robustness and insensitivity to parameter changes under different conditions. Given that a finer grid size of IMVDR corresponds to higher amplitude estimation accuracy and longer calculation time, a trade-off has to be made between higher amplitude accuracy and shorter calculation time.

3) The experimental results further verify that the proposed method can effectively extract the natural frequency of blades even in the non-resonance region and recover the complete frequency spectrum of blade vibration. Meanwhile, its anti-aliasing ability is better than other methods. When rotational speed fluctuates substantially, the performance of natural frequency identification may decrease owing to the change of array

steering matrix. However, natural frequency still appears in a certain frequency band.

At present, the high-precision estimation of amplitude remains a significant challenge for BHM. However, as an on-grid method, the estimation accuracy of frequency and amplitude with IMVDR will be limited by grid size, which is also an inevitable defect for almost all BTT spectrum recovery methods. In succeeding research, a more efficient and accurate co-correlation matrix estimation method suitable for the BTT signal should be introduced to further improve the accuracy of amplitude estimation.

Nomenclature

Abbreviations

ADMM	Alternating direction method of multipliers
BHM	Blade health monitoring
BTT	Blade tip timing
DoA	Direction of arrival
ESPRIT	Estimation of signal parameters via rotational invariance techniques
FEM	Finite element modeling
IMVDR	Improved minimum variance distortionless response
IRLS	Iteratively reweighted least squares
MUSIC	Multiple signal classification
MVDR	Minimum variance distortionless response
NUFT	Non-uniform Fourier transform
OMP	Orthogonal matching pursuit
OPR	Once per revolution
RMSE	Root mean square error
SNR	Signal-to-noise ratio
ToA	Time of arrival

Variables

a	Element of steering vector $\boldsymbol{a}$
$\boldsymbol{a}$	Steering vector
$\boldsymbol{a}_f$	Steering vector with tentative frequency f
$\boldsymbol{A}$	Array manifold matrix
$\boldsymbol{A}_x$	Array manifold matrix for signal measurement
c_i	Non-zero elements in the ith row of the matrix $\sqrt{\boldsymbol{S}/N}$
f	Frequency of synthetic signal
f_k	kth frequency in frequency grid
$\hat{f}_i^n$	ith estimated frequency in the nth Monte Carlo simulation
$f_\mathrm{r}(t)$	Blade's instantaneous rotation frequency at time t
$\bar{f}_\mathrm{r}(N_\mathrm{r})$	Blade averaged rotation frequency at the N_rth revolution
$(f_0, f_1, \ldots, f_{K-1})$	Frequency grid
$\{f_0', f_1', \ldots, f_{m-1}'\}$	Frequency set of the blade tip vibration
$\boldsymbol{G}$	Block matrix
$\boldsymbol{I}$	Identity matrix
K	Number of frequency grid
L	Length of the snapshot vector
m	Number of the frequencies in the input signal vector $\boldsymbol{x}(\boldsymbol{t}_n)$
M	Length of the input signal vector $\boldsymbol{x}(\boldsymbol{t}_n)$
n	Index of the first value
$\boldsymbol{n}(\boldsymbol{t}_n)$	Zero-mean additive noise vector
N, N_ite, N_max, N_mc, N_r	Numbers of the snapshots, iterations of MVDR, max iterations, Monte Carlo simulation, and the revolution, respectively
$P_{xx}(\boldsymbol{a})$	Power spectral density in steering vector $\boldsymbol{a}$
$P_{xx}(\boldsymbol{a}_f)$	Power spectral density in steering vector $\boldsymbol{a}_f$
$\hat{P}_{xx}(a_{f_k})$	Estimated power spectral density in steering vector $\boldsymbol{a}_{f_k}$
$\boldsymbol{P}_{xx}(\boldsymbol{A})$	Diagonal matrix in which diagonal elements represent the power spectral density
Q	Number of probes
R	Radius of the measurement point
$\boldsymbol{R}_i$	Correlation matrix of the ith snapshot
$\boldsymbol{R}_{xx}$	Correlation matrix of the signal x
$\hat{\boldsymbol{R}}_{xx}$	Estimated correlation matrix of the signal x
$\boldsymbol{R}'_{xx}$	Estimated correlation matrix of the signal x with spatial smoothing
s_{ij}	Element of the matrix $\sqrt{\boldsymbol{S}/N}$ in row i and column j
$\{s_0, s_1, \ldots, s_{m-1}\}$	Amplitude set of the blade tip vibration
$\boldsymbol{s}(\boldsymbol{t}_n)$	Vector of each frequency value at time $\boldsymbol{t}_n$
$\boldsymbol{S}$	Covariance matrix of $\boldsymbol{s}(\boldsymbol{t}_n)$
$\bar{\boldsymbol{S}}$	Spatial smoothed covariance matrix of $\boldsymbol{s}(\boldsymbol{t}_n)$
T_{n_r}	Time interval of adjacent pulses
t_act	Actual arrival time of the blade tip
t_exp	Expected arrival time of the blade tip
$\boldsymbol{t}_n$	Arrival time vector
$\boldsymbol{v}_i$	ith row of the Vandermonde matrix
w	Filter coefficient
$w(t)$	Filter coefficient at time t
$\boldsymbol{w}$	Filter coefficient vector
$\hat{\boldsymbol{w}}(\boldsymbol{a})$	Optimal filter coefficient vector
$\boldsymbol{W}$	Filter coefficient matrix
x	Input signal
$x(t)$	Vibration displacement of the blade at time t
$\boldsymbol{x}(\boldsymbol{t}_n)$	Input signal vector
$\boldsymbol{x}_i(\boldsymbol{t}_n)$	ith snapshots of input signal vector $\boldsymbol{x}(\boldsymbol{t}_n)$

$y(t_n)$	Output signal of the filter at time t_n
θ_q	Installation angle of the qth probe
$\Delta\theta$	Difference between two adjacent frequencies
ε	Error
σ_n^2	Variance of Gaussian white noise
λ	Regularization parameter of ADMM
ρ	Learning rate of ADMM
ω_0	Center frequency
$\{\varphi_0, \varphi_1, \ldots, \varphi_{m-1}\}$	Phase set of the blade tip vibration
$\mathbf{\Lambda}$	Diagonal matrix

Acknowledgements We are grateful for the support provided by the National Natural Science Foundation of China (Grant Nos. 52105117 and 51875433), and the Funds for Distinguished Young Talent of Shaanxi Province, China (Grant No. 2019JC-04).

Conflict of Interest The authors declare that they have no conflict of interest.

References

1. Oakley S Y, Nowell D. Prediction of the combined high- and low-cycle fatigue performance of gas turbine blades after foreign object damage. International Journal of Fatigue, 2007, 29(1): 69–80
2. Yang L H, Yang Z S, Mao Z, Wu S M, Chen X F, Yan R Q. Dynamic characteristic analysis of rotating blade with transverse crack—part I: modeling, modification, and validation. Journal of Vibration and Acoustics, 2021, 143(5): 051010
3. Yang L H, Yang Z S, Mao Z, Wu S M, Chen X F, Yan R Q. Dynamic characteristic analysis of rotating blade with transverse crack—part II: a comparison study of different crack models. Journal of Vibration and Acoustics, 2021, 143(5): 051011
4. Lawson C P, Ivey P C. Tubomachinery blade vibration amplitude measurement through tip timing with capacitance tip clearance probes. Sensors and Actuators A: Physical, 2005, 118(1): 14–24
5. Di Maio D, Ewins D J. Experimental measurements of out-of-plane vibrations of a simple blisk design using blade tip timing and scanning LDV measurement methods. Mechanical Systems and Signal Processing, 2012, 28: 517–527
6. Chana K S, Cardwell D N. The use of eddy current sensor based blade tip timing for FOD detection. In: Proceedings of the ASME Turbo Expo 2008: Power for Land, Sea, and Air. Berlin: ASME, 2008, 169–178
7. Russhard P. The rise and fall of the rotor blade strain gauge. In: Sinha J K, ed. Vibration Engineering and Technology of Machinery. Cham: Springer, 2015, 27–37
8. Kadambi J R, Quinn R D, Adams M L. Turbomachinery blade vibration and dynamic stress measurements utilizing nonintrusive techniques. Journal of Turbomachinery, 1989, 111(4): 468–474
9. Russhard P. Development of a blade tip timing based engine health monitoring system. Dissertation for the Doctoral Degree. Manchester: The University of Manchester, 2010
10. Kharyton V, Dimitriadis G, Defise C. A discussion on the advancement of blade tip timing data processing. In: Proceedings of the ASME Turbo Expo 2017: Turbomachinery Technical Conference and Exposition. Charlotte: ASME, 2017, V07BT35A002
11. Chen Z S, Sheng H, Xia Y M, Wang W M, He J. A comprehensive review on blade tip timing-based health monitoring: status and future. Mechanical Systems and Signal Processing, 2021, 149: 107330
12. Campbell W. Elastic-fluid turbine rotor and method of avoiding tangential bucket vibration therein. US Patent, 1502904, 1924-07-29
13. Zablotskiy I Y, Korostelev Y A. Measurement of Resonance Vibrations of Turbine Blades with the Elura Device. Technical Report NTIS 197915, 1978
14. Dimitriadis G, Carrington I B, Wright J R, Cooper J E. Blade-tip timing measurement of synchronous vibrations of rotating bladed assemblies. Mechanical Systems and Signal Processing, 2002, 16(4): 599–622
15. Carrington I B, Wright J R, Cooper J E, Dimitriadis G. A comparison of blade tip-timing data analysis methods. Proceedings of the Institution of Mechanical Engineers, Part G: Journal of Aerospace Engineering, 2001, 215(5): 301–312
16. Joung K K, Kang S C, Paeng K S, Park N G, Choi H J, You Y J, von Flotow A. Analysis of vibration of the turbine blades using non-intrusive stress measurement system. In: Proceedings of the ASME 2006 Power Conference. Atlanta: ASME, 2006, 391–397
17. Zhang Y G, Duan F J, Fang Z Q, Ye S H, Shi X H. Frequency identification technique for asynchronous vibration of rotating blades. Journal of Vibration and Shock, 2007, 12: 106–108, 174–175 (in Chinese)
18. Vercoutter A, Berthillier M, Talon A, Burgardt B, Lardies J. Estimation of turbomachinery blade vibrations from tip-timing data. In: Proceedings of the 10th International Conference on Vibrations in Rotating Machinery. London: Woodhead Publishing, 2012, 233–245
19. Donoho D L. Compressed sensing. IEEE Transactions on Information Theory, 2006, 52(4): 1289–1306
20. Lin J, Hu Z, Chen Z S, Yang Y M, Xu H L. Sparse reconstruction of blade tip-timing signals for multi-mode blade vibration monitoring. Mechanical Systems and Signal Processing, 2016, 81: 250–258
21. Wu S M, Zhao Z B, Yang Z B, Tian S H, Yang L H, Chen X F. Physical constraints fused equiangular tight frame method for blade tip timing sensor arrangement. Measurement, 2019, 145: 841–851
22. Li H Q, Yang Z B, Wu S M, Wang Z K, Tian S H, Yan R Q, Chen X F. Adaptive iterative approach for efficient signal processing of blade tip timing. IEEE Transactions on Instrumentation and Measurement, 2021, 70: 1–13
23. Chen S Y, Yang Y M, Hu H F, Guan F J, Shen G J, Bian Z F, Guo H N. Blind interpolation for multi-frequency blade tip timing signals. Mechanical Systems and Signal Processing, 2022, 172: 108946
24. Dong J N, Li H K, Fan Z F, Zhao X W, Wei D T, Chen Y G. Characteristics analysis of blade tip timing signals in synchronous resonance and frequency recovery based on subspace pursuit

algorithm. Mechanical Systems and Signal Processing, 2023, 183: 109632

25. Stéphan C, Berthillier M, Lardiès J, Talon A. Tip-timing data analysis for mistuned bladed discs assemblies. In: Proceedings of the ASME Turbo Expo 2008: Power for Land, Sea, and Air. Berlin: ASME, 2008, 447–455
26. Liu Z B, Duan F J, Niu G Y, Ye D C, Feng J N, Cheng Z H, Fu X, Jiang J J, Zhu J, Liu M R. Reconstruction of blade tip-timing signals based on the MUSIC algorithm. Mechanical Systems and Signal Processing, 2022, 163: 108137
27. Wang Z K, Yang Z B, Wu S M, Li H Q, Tian S H, Chen X F. An improved multiple signal classification for nonuniform sampling in blade tip timing. IEEE Transactions on Instrumentation and Measurement, 2020, 69(10): 7941–7952
28. Wang P, Karg D, Fan Z Y, Gao R X, Kwolek K, Consiglio A. Non-contact identification of rotating blade vibration. Mechanical Engineering Journal, 2015, 2(3): 15–00025
29. Capon J. High-resolution frequency-wavenumber spectrum analysis. Proceedings of the IEEE, 1969, 57(8): 1408–1418
30. Lacoss R T. Data adaptive spectral analysis methods. Geophysics, 1971, 36(4): 661–675
31. Benesty J, Chen J D, Huang Y T. A generalized MVDR spectrum. IEEE Signal Processing Letters, 2005, 12(12): 827–830
32. Liepin'Sh V Y. An algorithm for evaluating a discrete Fourier transform for incomplete data. Automatic Control and Computer Sciences, 1996, 30: 20–29
33. Shan T J, Wax M, Kailath T. On spatial smoothing for direction-of-arrival estimation of coherent signals. IEEE Transactions on Acoustics, Speech, and Signal Processing, 1985, 33(4): 806–811
34. Wu S M, Russhard P, Yan R Q, Tian S H, Wang S B, Zhao Z B, Chen X F. An adaptive online blade health monitoring method: from raw data to parameters identification. IEEE Transactions on Instrumentation and Measurement, 2020, 69(5): 2581–2592
35. Greitans M. Multiband signal processing by using nonuniform sampling and iterative updating of autocorrelation matrix. In: Proceedings of the 2001 International Conference on Sampling Theory and Application. Orlando, 2001, 85–89
36. Pati Y C, Rezaiifar R, Krishnaprasad P S. Orthogonal matching pursuit: recursive function approximation with applications to wavelet decomposition. In: Proceedings of the 27th Asilomar Conference on Signals, Systems and Computers. Pacific Grove: IEEE, 1993, 40–44
37. Bouchain A, Picheral J, Lahalle E, Chardon G, Vercoutter A, Talon A. Blade vibration study by spectral analysis of tip-timing signals with OMP algorithm. Mechanical Systems and Signal Processing, 2019, 130: 108–121
38. Boyd S, Parikh N, Chu E, Peleato B, Eckstein J. Distributed optimization and statistical learning via the alternating direction method of multipliers. Now Foundations and Trends, 2011, 3(1): 1–122
39. Stoica P, Li H, He H. Spectral analysis of nonuniformly sampled data: a new approach versus the periodogram. IEEE Transactions on Signal Processing, 2009, 57(3): 843–858
40. Hajnayeb A, Nikpour M, Moradi S, Rossi G. A new reference tip-timing test bench and simulator for blade synchronous and asynchronous vibrations. Measurement Science & Technology, 2018, 29(2): 025203
41. Beauseroy P, Lengellé R. Nonintrusive turbomachine blade vibration measurement system. Mechanical Systems and Signal Processing, 2007, 21(4): 1717–1738
42. Wang Z K, Yang Z B, Li H Q, Cao J H, Tian S H, Chen X F. Automatic tracking of natural frequency in the time–frequency domain for blade tip timing. Journal of Sound and Vibration, 2022, 516: 116522